Quantification of the Flexibility of Residential Prosumers

István G. Balázs *, Attila Fodor [ID] **and Attila Magyar** [ID]

Department of Electrical Engineering and Information Systems, University of Pannonia, Egyetem str. 10., H-8200 Veszprém, Hungary; foa@almos.uni-pannon.hu (A.F.); magyar.attila@virt.uni-pannon.hu (A.M.)
* Correspondence: balazs.istvan@virt.uni-pannon.hu

Abstract: Balancing in a distributed generation network is an increasingly difficult task because of the increasing number of residential prosumers on the power network. This paper proposes a framework for the estimation, as well as the prediction of the power flexibility of residential prosumers. In order to quantify the residential buildings' demand flexibility, a thermoelectric simulation model of a typical residential house was developed based on first engineering principles. Based on the calculated flexibility values, a simple prediction method was used to give a short-term forecast of the prosumer flexibility. The results were validated by simulation experiments incorporating real data for four different scenarios.

Keywords: flexibility; demand response; distributed generation

1. Introduction

In the past, conventional power systems were characterized by large generation sources that injected power into the transmission grid, which was transported to distribution networks and then delivered to the end-users. Power flowed one way from the high-voltage transmission grid to the end-user at low-voltage networks. Centralized, dispatchable, and predictable generation provided flexibility at the transmission level to the electric system to balance generation and demand, implementing a generation-follows-load paradigm [1].

The increasing amount of distributed and renewable generation (from around a 21% share of net power generation in 2010 to 44% in 2030 [2]) transforms the generation side into a more variable and intermittent source of energy, so the forecast and control of the solar [3] and wind [4] energy production represent a handful of problems. With the emergence and significant increase of the distributed and intermittent generation share, the generation-follows-load paradigm has become unsustainable. The integration of renewable resources poses new challenges for both the TSO responsible for frequency regulation and the DSO responsible for the operation of the distribution network. Progress has been made to increase the predictability [5] and controllability [6,7] of renewables, but the involvement of the demand-side and load-follows-generation models are inevitable. On the one hand, the penetration of intermittent generation and distributed energy resources has already forced TSOs (transmission system operators) to increase the volume of balancing capabilities and start procuring services for system balancing, not only from the transmission grids, but also from the distribution grids. On the other hand, DSOs have also been empowered to acquire flexibility services, to control the production and consumption of system users. In addition to the quantitative reason, the voltage level, power flow direction, and network congestion problems arising in medium- and low-voltage networks can be handled locally, so the network location becomes more important.

Flexibility is the modification of generation injection and/or consumption patterns in reaction to an external signal (price signal or activation) in order to provide a service within the energy system [8,9]. It is the active management of an asset that can impact system balance or grid power flows on a short-term basis. The proper management of

available flexibility, both on generation and the demand-side, can help to compensate for the lack of certainty of renewable sources. As variable renewable energy sources constitute a larger fraction of electricity supply, interest in flexible resources [10], including demand response, dispatchable generation, transmission interconnection, and storage technologies, is growing. In the near future, demand-side flexibility would be required for managing power grids. Buffered heat pumps (HPs) are examples of domestic hot water (DHW) systems and stationary batteries for flexible residential loads that can store energy from the grid and local generators (e.g., solar panels). Both forms of stored energy (thermal or chemical) can be used to support self-consumption.

Building energy systems will serve as one possible source of demand-side energy flexibility. Traditionally, buildings have been consumers of energy, but they are responsible for a large share of energy demand and therefore may play a key role in improving the flexibility in the demand-side of the entire energy system.

The size of a residential household does not reach the volume to be able to bid on energy markets independently, so prosumers may share their flexibility with a pool. The flexibility pool is managed by an aggregator [11], which can be a DSO, a TSO, or an independent intermediary entity. Whatever market design is implemented, the prosumer receives a premium as compensation for the provided flexibility from the aggregator [12]. The results of [13] showed that the aggregator is able to find a match between the flexibility provisioned and the flexibility procured by the DSO. The aggregator reduces the remuneration costs paid to users for the flexibility at the same time. The aggregator bids on energy markets aggregating prosumers' flexibility, so it needs to have information about the flexibility volume of the pool. Either the prosumer provides a bid or the aggregator bears the risk; therefore, the amount of flexibility must therefore be quantified, and a function has to exist to predict the available flexibility.

1.1. Literature Review

In the example of [14], extrapolating the Belgian national level implied that domestic flexibility could equal 1.8% (upward) and 12.1% (downward) of installed generation capacity. The results presented by the authors of [15] forecast that the household sector will be able to contribute significantly to the distribution system stabilization with an average potential of 30 GW downwards and 3 GW upwards flexibility in the year 2025. Paper [15] analyzed the potential that is made possible by technology for the provision of system services by households. Single-family and twin homes were the main focus, since those are the types of households in which all system components are available. The Electric Power Research Institute (EPRI) estimated a technical potential summer peak reduction of 175GW from demand response by 2030 in the USA [16]. The Clean Energy for All Europeans Package (CEP) [17] empowers prosumers in the EU to offer their flexibility. The volume necessary for energy markets requires a large number of prosumers to participate in energy services. Energy companies require digitalization and the utilization of advanced technologies [18], as well as market models [19] to involve prosumers in the electricity markets. Using blockchain technology can simplify the management of microgrid power transactions and realize peer-to-peer power transactions [20].

The technical potential of demand modification profiles was presented for different regions in the USA in [16]. There are six different load curves of the demands of residential users [21], for which the demand-side management (DSM) techniques are the following: peak clipping, valley filling, load shifting, load reduction, load growth, and flexible load shape. The flexible load shape technique was assumed in this paper.

Paper [22] proposed an energy storage system as a possible flexibility resource and its potential role in the future smart grid network. The potential benefits of energy storage as the flexibility resource can facilitate increased participation of storage in different electricity markets and improve the flexibility of smart grid operation with a high penetration of renewable energy sources. Paper [23] analyzed the potential of grid flexibility supply by combined heat and power systems installed at business facilities. Simulations were

performed for a representative day in each season and four types of facilities. Prosumer systems can operate both an autonomous (off-grid) and grid-connected (on-grid) systems. While the energy generated in autonomous systems is consumed by the system's own consumption devices, the energy produced in grid-connected systems can be consumed by the system internally, or if there is energy surplus, it can supply the grid [24].

The flexibility of industrial prosumers is a widely researched area with several outstanding results and papers [25,26]; however, with the advent of the smart grid, this is increasingly complemented by the flexibility of residential actors. Residential prosumers form a promising source of flexibility due to their distributed location and substantial share of the electricity market. Home energy management (HEM) systems can reduce electricity consumption by scheduling electrical appliances [27]. There are several control strategies and methods for HEM: AI-based control (predictive control, optimization control), linear online control, and storage systems.

Quantifying flexibility is challenging due to its complex electrothermal dynamics and time delay effects in general. Methodologies to quantify the energy flexibility of buildings are affected by the definition of flexibility followed by the respective research. A summary of quantification methods for the energy flexibility of buildings was provided by [28], in which the characterization of energy flexibility was a demand increase/generation decrease as negative flexibility and a demand decrease/generation increase as positive flexibility. The methodology proposed by [29] considers the flexibility of a specific system as the ability to shift the consumption of a certain amount of electrical power in time. Reference [30] defined flexibility as the possibility to change the electricity consumption of a building from the reference scenario at a specific point in time and during a certain time span. The quantification of flexibility from a district heating system point of view was given in [31]. The district heating system was firstly decomposed into multiple parallel subsystems with simpler topological structures. The maximum flexibility of each subsystem was then formulated as a delayed optimal control problem, and finally, the available flexibility from the original system was estimated by aggregating the flexibility of all subsystems.

In [32], household devices were categorized as shifted, but not varied, shifted and varied, and not shifted, but varied. The simulation results showed that the flexibility of houses under testing had maximum power values of 200–500 W. The authors of [33] described the customer-side time flexibility with respect to white goods (washing machine, dryer, dish washer) with two parameters: configuration time and deadline. The paper modeled customer flexibility behavior with finite mixture models.

1.2. Aim and Contribution

The *research question* of our study is whether it is possible to calculate and forecast the up and down flexibility of a residential house based on measurable quantities. A model-based approach was applied to simulate the energy processes of a residential building, in which the electrical devices were modeled and power consumption/generation was calculated for each device, so that the consumption/generation modification opportunities could be defined as the prosumer's flexibility. By configuring the external parameters of the model, the energy consumption of the house and the available flexibility could be simulated for different scenarios. A supervised prediction could be built on it, in which the simulation produced flexibility as a dependent variable. The prosumer model could be scaled to a pool of prosumers that could provide flexibility inputs for an aggregator function.

The contribution of this paper can be summarized in three main points. First of all, a dynamic model of a typical residential building energy system is developed based on first engineering principles. The simulation model was implemented in the MATLAB Simulink environment. On the other hand, a calculation scheme is given for determining the flexibility of residential houses. Finally, a prediction method was developed and implemented in the Python environment to provide a 15 min forecast of the prosumer flexibility.

1.3. Structure of the Paper

The structure of the paper is as follows. After assessing the state-of-the-art in the proposed research area in the present section, the modeling assumptions and the structure of the proposed residential prosumer model are detailed in Section 2, and based on it, a simulation-based case study is presented in Section 3. This is followed by Section 4, which summarizes and concludes the paper.

2. Modeling and System Structure

For the study of demand flexibility, a residential building was assumed that is located in Hungary. The building is equipped with an electric heating system, a separate water heater, a home energy storage system, and rooftop PV panels (see Figure 1).
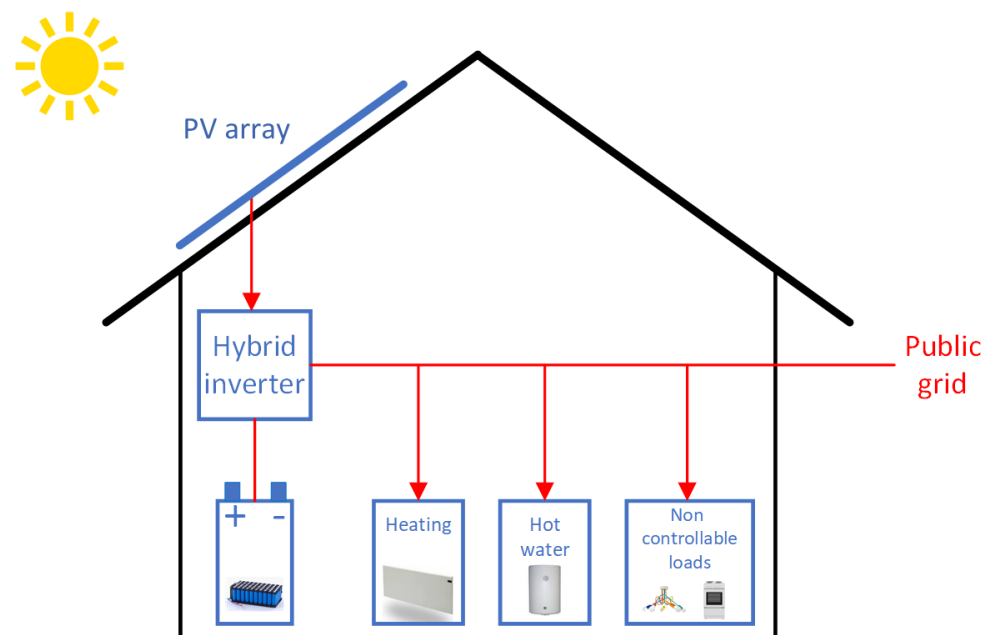

Figure 1. High-level model of the system. Line segments without arrow heads represent bidirectional power flow.

The prosumer model consisted of energy consumers (space heater, hot water, and noncontrollable load), a producer (PV), and a battery. The house was connected to the grid (on-grid mode), and power flow was available in both directions. All the energy needs of the house were supplied by the PV panels and the grid, and there was no other source of power (e.g., gas, central heating). Besides using energy from the grid, the PV panels and the battery can also supply the consumers. When available, self-consumption is preferred. Instantaneous flexibility was calculated for all the devices in both directions and summed to provide a time series of the available flexibility.

A thermal model was developed for the space heating and hot water system. Not every electrical appliance can be controlled without inconveniencing consumers, so there are some appliances that consumers may always need access to. The flexibility of these appliances (e.g., lights, water, kitchen devices, other household appliances) was not considered in this study; their consumption is referred to as noncontrollable load. Power was supplied from the PV system, energy storage, or the grid. A conventional greedy algorithm was implemented to control energy storage operation when no external flexibility regulation was applied. The objective was to minimize grid usage.

There was no need for a separate flexibility control block in the case of the default operation scenario, when no external flexibility activation occurs. All the dispatchable devices could operate autonomously, and the greedy implementation of battery operation required no central control logic. Flexibility was calculated for each device, and the

sum represents the available flexibility of the house for both the up and down direction. Flexibility followed the interpretation proposed by the authors of [28], i.e., it was assumed to be a signed value, positive when generation can be increased or consumption can be decreased and negative in the case when generation can be decreased or consumption can be increased.

The residential house of the case study has the parameters presented in Table 1.

Table 1. Exogenous variables of the system.

Parameter	Description	Unit
m_{water}	mass of water in the tank	kg
$T_{water}(0)$	initial water temperature	°C
T_{water}^{sp}	water temperature setpoint	°C
T_{water}^{th}	water temperature threshold	°C
$dm_{water}^{cons}(t)/dt$	water consumption	kg/s
C_{water}	heat capacity of air (273 K)	J/(kg·K)
η_{water}	efficiency of the water heater	-
P_{water}^{max}	power capacity of the water heater	W
hl_{water}	heat loss rate	W/(kg · K)
l_H	length of the house	m
w_H	width of the house	m
h_H	height of the house	m
n_W	number of windows	-
w_W	width of a window	m
h_W	height of a window	m
λ_{Brick}	thermal conductivity of brick	W/(m·K)
λ_{EPS}	thermal conductivity of EPS insulation	W/(m·K)
d_{Brick}	brick thickness	m
d_{InsW}	insulation thickness of the walls	m
d_{InsS}	insulation thickness of the slab	m
$U_{Windows}$	heat transfer coefficient of the windows	W/(m²·K)
$T_{air}^{indoor}(0)$	initial indoor air temperature	°C
$T_{air}^{outdoor}(t)$	outdoor temperature	°C
T_{air}^{sp}	air temperature setpoint	°C
T_{air}^{th}	air temperature threshold	°C
$T_{heating}$	temperature of air exiting the heater	°C
$dm_{air}(t)/dt$	air flow rate of the heater	kg/s
C_{air}	heat capacity of air (273 K)	J/(kg·K)
ρ_{air}	density of air at sea level	kg/m³
$P_{heating}^{max}$	maximum power capacity of the heater	W
$cop_{heating}$	heating system's coefficient of performance	-
$SoC(0)$	battery initial state-of-charge	%
$MinSoC$	battery minimum state-of-charge	%
$MaxSoC$	battery maximum state-of-charge	%
$P_{battery}^{max}$	maximum power of the battery	W
$\eta_{battery}$	efficiency of the battery	-
$P_{pv}(t)$	power generation of the PV panels	W
$P_{load}(t)$	power consumption of the noncontrollable load	W

2.1. Hot Water

Hot water is supplied by an electric water tank containing m_{water} kilograms of water. A setpoint (T_{water}^{sp}) specifies the maximum temperature of the water, and a thermostat controls the heating cycles. The thermostat switches the heater off at the setpoint and turns it on (Equation (2)) when the temperature drops below the setpoint by a threshold value

(T_{water}^{th}). When the heater is on, a heating wire warms up the water by η_{water} efficiently consuming a constant level of power (P_{water}).

A water tank model calculates the water temperature dynamics (Equation (1)). The water temperature change ($\frac{dT_{water}(t)}{dt}$) has three main inputs: heat provided by the heater ($\frac{dQ_{water}^{gain}(t)}{dt}$), hot water consumption ($\frac{dQ_{water}^{cons}(t)}{dt}$), and heat losses ($\frac{dQ_{water}^{heatloss}(t)}{dt}$). When hot water is consumed, the same amount of cold water ($\frac{dm_{water}^{cons}(t)}{dt}$) fills the tank. The inflow water temperature is the same as the outside temperature ($T_{air}^{outdoor}(t)$); thus, consumption cools the tank. The heat outflow is proportional to the temperature difference between the cold and the tank water ($T_{water}(t)$). Heat loss is calculated considering a heat loss parameter (hl_{water}) [34] and the difference between water and room temperature (T_{air}^{indoor}). The room temperature is an output signal of the heating subsystem.

The energy balance of the hot water subsystem is expressed by the following equations:

$$
\begin{aligned}
Cons_{water}(t) &= P_{water}^{max} \cdot Reg_{water}(t) \\
\frac{dQ_{water}^{gain}(t)}{dt} &= Cons_{water}(t) \cdot \eta_{water} \\
\frac{dQ_{water}^{cons}(t)}{dt} &= (T_{water}(t) - T_{air}^{outdoor}(t)) \cdot \frac{dm_{water}^{cons}(t)}{dt} \cdot C_{water} \\
\frac{dQ_{water}^{heatloss}(t)}{dt} &= (T_{water}(t) - T_{air}^{indoor}) \cdot m_{water} \cdot hl_{water} \\
\frac{dT_{water}(t)}{dt} &= \left(\frac{dQ_{water}^{gain}(t)}{dt} - \frac{dQ_{water}^{cons}(t)}{dt} - \frac{dQ_{water}^{heatloss}(t)}{dt} \right) \frac{1}{m_{water} \cdot C_{water}}
\end{aligned}
\tag{1}
$$

where $Cons_{water}(t)$ stands for the actual water consumption of the house.

$$
Reg_{water}(t) = \begin{cases} 1 & \text{, when the water heater is on,} \\ 0 & \text{, when the water heater is off.} \end{cases}
\tag{2}
$$

Power is a signed value. $P_{water}(t)$ is negative (consumption) when the heater is on ($Reg_{water}(t)$):

$$
P_{water}(t) = -Cons_{water}(t).
\tag{3}
$$

The calculated flexibility can be defined for both the up and down direction between current power consumption and the maximum power capacity (down) or 0 (up) using (Equation (4)) below.

$$
\begin{aligned}
F_{water}^{up}(t) &= Cons_{water}(t) \\
F_{water}^{down}(t) &= Cons_{water}(t) - P_{water}^{max}
\end{aligned}
\tag{4}
$$

2.2. Heating

The thermal model of a house calculates the power consumption of the heating system that keeps the indoor temperature around a defined setpoint. The heating system is equipped with a thermostat and an electric heater. Similar to the water heater, the thermostat switches the heater on and off (Equation (9)) when the temperature drops below and above the setpoint (T_{air}^{sp}) by a predefined threshold (T_{air}^{th}). An air-to-air heat pump supplies warm air for the house, operating at an average COP ratio ($cop_{heating}$).

Total thermal resistance (R_{tot}) is calculated from the geometry and the material properties of the house (Equation (5)). The walls of the house are made of bricks, and EPS insulation is used on the walls and the slab.

$$
\begin{aligned}
A_{Windows} &= n_W \cdot h_W \cdot w_W \\
A_{Walls} &= 2 \cdot l_H \cdot h_H + 2 \cdot w_H \cdot h_H - A_{Windows} \\
A_{Slab} &= w_H \cdot l_H \\
A &= A_{Windows} + A_{Walls} + A_{Slab}
\end{aligned}
\tag{5}
$$

The thermal resistance of thermally homogeneous components is calculated using (Equation (6)).

$$
\begin{aligned}
R_{Windows} &= 1/U_{Windows} \\
R_{Walls} &= d_{Brick}/\lambda_{Brick} + d_{InsW}/\lambda_{EPS} \\
R_{Slab} &= d_{InsS}/\lambda_{EPS}
\end{aligned}
\tag{6}
$$

The total thermal resistance (R_{tot}) is determined by assuming one-dimensional heat flow perpendicular to the walls. It is given (Equation (7)) by the method in the ISO 6946/2007 standard [35].

$$
R_{tot} = \frac{A}{A_{Walls}/R_{Walls} + A_{Windows}/R_{Windows} + A_{Slab}/R_{Slab}}
\tag{7}
$$

A thermal model calculates the indoor air temperature dynamics of the house. Its two main inputs are the heat provided by the heating system and heat losses. Contrary to the water heater, heat gain ($\frac{dQ_{heating}^{gain}(t)}{dt}$) is not persistent, but proportional to the temperature difference between the room (T_{air}^{indoor}) and the constant heated air temperature ($T_{heating}$). Heat loss ($\frac{dQ_{heating}^{heatloss}(t)}{dt}$) is proportional to the temperature difference between the room and outdoor temperature ($T_{air}^{outdoor}$). The indoor temperature time derivative ($\frac{dT_{air}^{indoor}(t)}{dt}$) is expressed by the following equations:

$$
\begin{aligned}
\frac{dQ_{heating}^{gain}(t)}{dt} &= \min\left((T_{heating} - T_{air}^{indoor}(t))\frac{dm_{air}(t)}{dt}C_{air}, P_{hp}^{max}cop_{heating} \right) Reg_{heating}(t) \\
\frac{dQ_{heating}^{heatloss}(t)}{dt} &= \left(T_{air}^{indoor}(t) - T_{air}^{outdoor}(t) \right)\frac{1}{R_{tot}}A \\
\frac{dT_{air}^{indoor}(t)}{dt} &= \left(\frac{dQ_{heating}^{gain}(t)}{dt} - \frac{dQ_{heating}^{heatloss}(t)}{dt} \right)\frac{1}{(l_H \cdot w_H \cdot h_H) \cdot \rho_{air} \cdot C_{air}}
\end{aligned}
\tag{8}
$$

$$
Reg_{heating}(t) = \begin{cases} 1 & \text{, when the heater is on,} \\ 0 & \text{, when the heater is off.} \end{cases}
\tag{9}
$$

$Cons_{heating}(t)$ denotes a theoretical power consumption that is necessary to warm the indoor air up to the constant heated air temperature.

$$
Cons_{heating}(t) = \min\left(\frac{(T_{heating} - T_{air}^{indoor}(t))\frac{dm_{air}(t)}{dt}C_{air}}{cop_{heating}}, P_{hp}^{max} \right)
\tag{10}
$$

Power is a signed value. $P_{heating}(t)$ is negative (consumption) when the heater is on:

$$P_{heating}(t) = -Cons_{heating}(t)Reg_{heating}(t). \tag{11}$$

The available flexibility quantity from the heating system is calculated for both directions (Equation (12)). When the heater is on, its power consumption can be decreased, and the maximum upward flexibility is the difference between instantaneous power and zero. When it is off, downward regulation is available by turning the heater on.

$$F_{heating}^{up}(t) = Cons_{heating}(t)Reg_{heating}(t) \tag{12}$$
$$F_{heating}^{down}(t) = -Cons_{heating}(t)(1 - Reg_{heating}(t))$$

2.3. Storage

Storage provides the flexibility of shifting energy over time. A conventional greedy algorithm was implemented to control the storage operation when no external flexibility regulation was applied [36] in order to prefer self-consumption and reduce feed-in power. If there is a higher consumption by the household than generation by the PV, the storage is discharged until a minimum charge level. When generation surplus occurs, the storage is charged until it is full.

The storage model (Equations (13)–(16)) processes the power requirement ($Reg_{battery}(t)$), determines the default storage operation (charge: $Cons_{battery}^{charge}(t)$/discharge: $Cons_{battery}^{discharge}(t)$), and calculates current state-of-charge ($SoC(t)$) taking into consideration the power limits ($P_{battery}^{max}$), capacity limits ($MinSoC, MaxSoC$), and efficiency ratio ($\eta_{battery}$).

$$Reg_{battery}(t) = P_{water}(t) + P_{heating}(t) + P_{load}(t) + P_{pv}(t) \tag{13}$$

$$Cons_{battery}^{charge}(t) = \begin{cases} \min(\max(0, Reg_{battery}(t)), P_{battery}^{max}), & \text{when } SoC(t) < MaxSoC, \\ 0, & \text{otherwise} \end{cases} \tag{14}$$

$$Cons_{battery}^{discharge}(t) = \begin{cases} \max(\min(0, Reg_{battery}(t)), -P_{battery}^{max}), & SoC(t) > MinSoC, \\ 0, & \text{otherwise} \end{cases} \tag{15}$$

$$\frac{dSoC(t)}{dt} = \frac{Cons_{battery}^{charge}(t) \cdot \eta_{battery} + Cons_{battery}^{discharge}(t) \cdot (2 - \eta_{battery})}{Cap} \tag{16}$$

The battery's contribution to the net power balance of the house ($P_{battery}(t)$) has the opposite sign of battery consumption.

$$P_{battery}(t) = -Cons_{battery}^{charge}(t) - Cons_{battery}^{discharge}(t) \tag{17}$$

Given the maximum charge ($P_{battery}^{max}$) and discharge ($P_{battery}^{min}$) power of the energy storage and the instantaneous power output, both up and down regulation capacity can be calculated ($F_{battery}^{up}(t), F_{battery}^{down}(t)$) when the state-of-charge is between the charge limits.

$$F_{battery}^{up}(t) = P_{battery}^{max} - P_{battery}(t) \tag{18}$$
$$F_{battery}^{down}(t) = -P_{battery}^{max} - P_{battery}(t)$$

2.4. Noncontrollable Load

The consumption of the household is made up of controllable and noncontrollable loads. While the controllable load was presented in the previous sections, the measured data were used for the noncontrollable load time series ($P_{load}(t)$). No flexibility was available for the noncontrollable load.

2.5. PV Generation

PV generation ($P_{pv}(t)$) depends only on solar radiation. When no flexibility control was applied, it was assumed that the panels always generated the maximum power, and no upward regulation was available. The PV can offer downward flexibility ($F_{pv}^{down}(t)$) between 0 and its current generation.

$$F_{pv}^{down}(t) = -P_{pv}(t) \tag{19}$$

2.6. Power Balance and Total Flexibility

The power balance of the house is calculated by summarizing the signed values of each component.

$$P_{balance}(t) = P_{water}(t) + P_{heating}(t) + P_{battery}(t) + P_{load}(t) + P_{pv}(t) \tag{20}$$

The total flexibility is calculated separately for the up and down direction:

$$F_{total}^{up}(t) = F_{water}^{up}(t) + F_{heating}^{up}(t) + F_{battery}^{up}(t)$$
$$F_{total}^{down}(t) = F_{water}^{down}(t) + F_{heating}^{down}(t) + F_{battery}^{down}(t) + F_{pv}^{down}(t) \tag{21}$$

2.7. Model Verification

The simulation parameters were configured taking the geometry and materials used in the well-insulated, single-story residential house built in 2015 in Hungary. The building has a ground floor area of 172 m^2, made of insulated brick (38 + 15 cm). The ceiling has a concrete structure with 30 cm of insulation. The windows have three-pane thermal insulated glazing.

The parameters and calculated variables were compared to the values of the single-family house involved in the IEA EBC Annex 58 project [37]. The referenced building area is 100 m^2; its brick walls are insulated, and double-pane windows were built in. The benchmark building has slightly worse U-values [38], but the total conductance is lower, because of the difference in size. Interior walls were also considered in the thermodynamic calculations. The comparisons of the heat transfer coefficients are given in Table 2.

Table 2. Calculated heat transfer coefficients.

Component	Building in the Present Study	Building in the IEA EBC Annex 58 Project	Unit of Measure
External walls	0.16	0.2	W/(m^2·K)
Windows	0.9	1.12	W/(m^2·K)
Slab	0.12	0.17	W/(m^2·K)
Total envelope conductance	57	36.6	W/K

The model was tested with manual inputs. Figure 2 shows the model response for an arbitrarily chosen input set. In the beginning, there was no consumption. PV generation ramped up to 4 kW. It charged the battery and supplied the load between one and two. The power balance of the house remained zero until the battery was full. At Hour 5, the outdoor temperature dropped to −2 °C from 24 °C, making the space heater turn on after 40 min. Between Hours 6 and 8, 6 L/min hot water was also used. The battery supplied

the noncontrollable load and the consumption of both heaters until the SoC reached its minimum level. The building was fed from the grid after Hour 8. It can be concluded that the proposed simulation model corresponded to the engineering expectations.
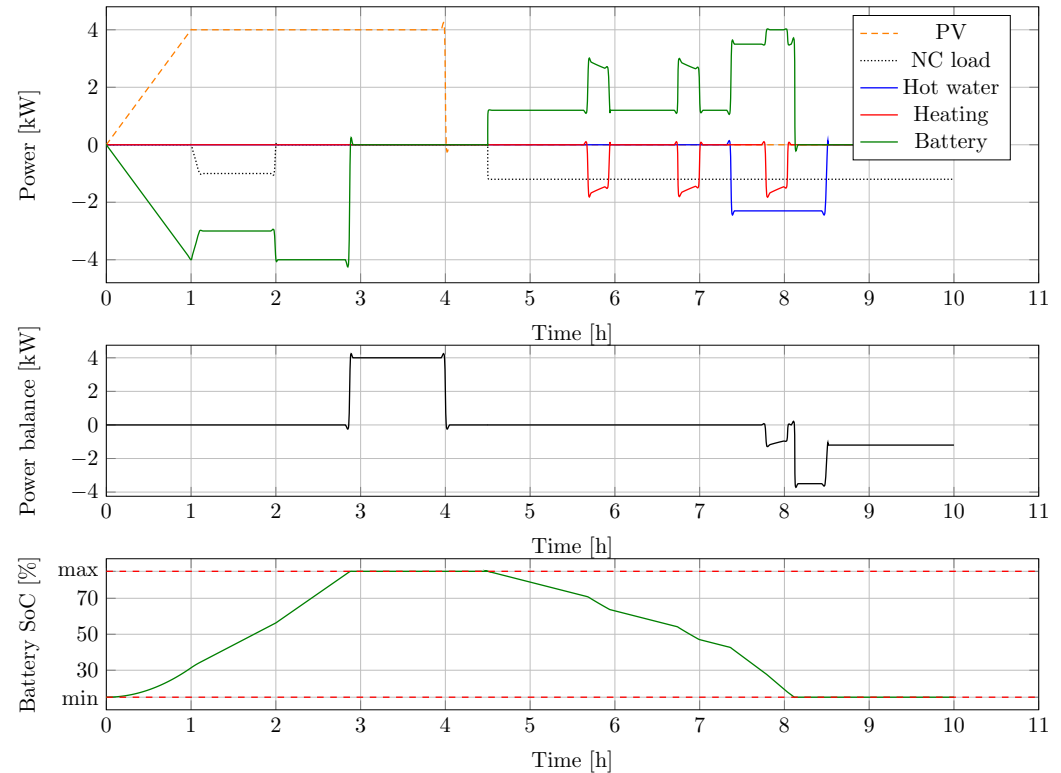

Figure 2. Power of the devices for the verification inputs.

2.8. Flexibility Prediction

The quantification of the flexibility provides instant volumes of the up and down regulation capabilities. Instantaneous values are not valuable for flexibility buyers such as system operators, so forecasts need to be calculated. It was not a primary objective of this paper to study the prediction methods and evaluate the results; however, a simple forecast model was built to show the short-term prediction opportunities.

A linear model was fit to minimize the residual sum of squares between the observed features and the values predicted by the linear approximation. Ridge regression was used, which kept all predictors in the model, but performed an L2-norm regularization, reducing the impact of correlated predictors. Ridge regression is a regularized version of linear regression where a regularization term is added to the cost function. This forces the learning algorithm to not only fit the data, but also keep the model weights smaller in magnitude [39]. The objective function of RR is defined as follows [40]:

$$\min_{\boldsymbol{w}} \frac{1}{2} \sum_{i=1}^{n} ||\boldsymbol{w}^T \boldsymbol{x}_i - y_i||_2^2 + \lambda ||\boldsymbol{w}||_2^2, \tag{22}$$

where $\boldsymbol{x}_i$ is the feature vector of the i-th sample and y_i is the independent variable's true value. λ is a regularization parameter. Weight vector $\boldsymbol{w}$ is calculated by taking the derivative of Equation (22) and setting it to zero.

$$\boldsymbol{w} = (\boldsymbol{X}\boldsymbol{X}^T + \lambda \boldsymbol{I})^{-1}\boldsymbol{X}\boldsymbol{y}^T \tag{23}$$

A 15 min interval is the typical market time unit for settlement in the energy sector in Europe. The calculation of a 15 min forecast of upward flexibility assumes that it has a linear relationship between upward flexibility (y_i) and the predictor variables ($\boldsymbol{x}_i$). PV

generation, heating system/water heater consumption, power, and the state-of-charge of the battery were selected as the explanatory variables. There was no prediction of the features, so 15 min lags were applied to construct the predictor set (Equation (25)). A 15 min average of the target variable was calculated and lagged by 15 min (Equation (24)).

$$Flex_{rolling}^{up}(i) = \frac{\sum_{t=i-18001200}^{i-900300} F_{total}^{up}(t)}{900} \tag{24}$$

$$\mathbf{x}_i = \begin{bmatrix} P_{water}(i-900) \\ P_{heating}(i-900) \\ P_{battery}(i-900) \\ P_{pv}(i-900) \\ SoC(i-900) \\ Flex_{rolling}^{up}(i) \end{bmatrix} \tag{25}$$

Ridge regression puts constraints on the size of the coefficients associated with each variable. These values depend on the magnitude of each variable. If a variable is measured at a higher scale than the other variables and not centered around zero, they do not give an equal contribution to the analysis. Both the training and test set must be standardized based on the mean and standard deviation learned from the training set by removing the mean and scaling data to unit variance as follows:

$$z = \frac{x - \mu}{\sigma}, \tag{26}$$

where μ is the mean, σ is the standard deviation of x, and z is the scaled predictors.

The coefficient of variation of the root-mean-squared error (CVRMSE) and the coefficient of determination (R^2 score) were used as a set of criteria to evaluate the prediction. The CVRMSE (Equation (27)) measures the variability of errors between true and predicted values. It gives an indication of the model's ability to predict the overall load shape that is reflected in the data [41].

$$CVRMSE(y, \hat{y}) = \frac{1}{\frac{1}{n}\sum_{i=1}^{n} y_i} \sqrt{\frac{1}{n}\sum_{i=1}^{n}(y_i - \hat{y}_i)^2} 100 \tag{27}$$

R^2 (28) represents the proportion of variance that has been explained by the independent variables in the model. It provides an indication of the goodness of fit and therefore a measure of how well unseen samples are likely to be predicted by the model, through the proportion of explained variance [42].

$$R^2(y, \hat{y}) = 1 - \frac{\sum_{i=1}^{n}(y_i - \hat{y}_i)^2}{\sum_{i=1}^{n}(y_i - \bar{y})^2}, \tag{28}$$

where:
- n: number of samples;
- y_i: true value;
- $\hat{y}_i$: predicted value of the i-th sample;
- $\bar{y} = \frac{1}{n}\sum_{i=1}^{n} y_i$.

3. Case Study and Results

3.1. Scenarios

The energy model of the house in Section 2 was implemented in MATLAB Simulink. It calculated the total power consumption/generation and available flexibility that it could offer. Four simulations were performed to analyze flexibility under different weather conditions and patterns for a 24 h period. The scenarios differed in the PV generation and

outer temperature time series data, and it was assumed that the noncontrollable load and water consumption patterns were the same in each scenario. Please refer to Appendix A to review additional parameter values.

Figure 3 shows the difference between the solar generation profile for the different scenarios. The 1 min measurements from a 400 kVA PV park were collected and normalized by the peak power capacity. The relative production of each scenario was multiplied by the capacity of the modeled rooftop panels to obtain the PV generation time series ($P_{pv}(t)$).
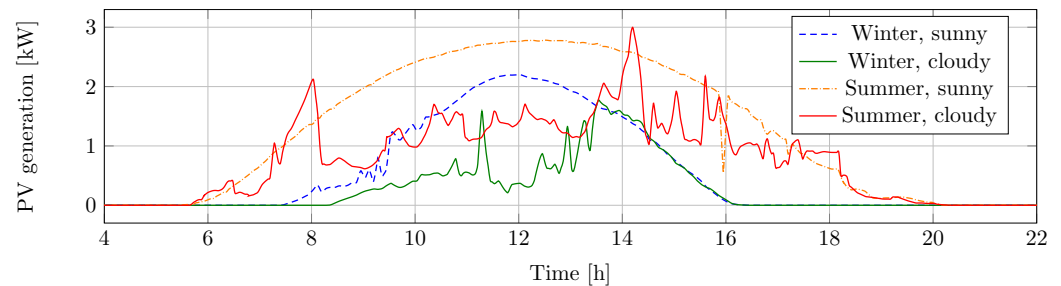
Figure 3. PV generation profiles for the four scenarios. The higher generation at 8 a.m. on a cloudy summer day (red line) compared to a sunny summer day (orange, dashed) comes from the efficiency increase caused by the cooling (a possible cloud passing by) at 7 a.m.

Figure 4 shows the environmental temperature (T_{out}) for the different scenarios. Temperature data were collected from the PV site ($T_{air}^{outdoor}(t)$).
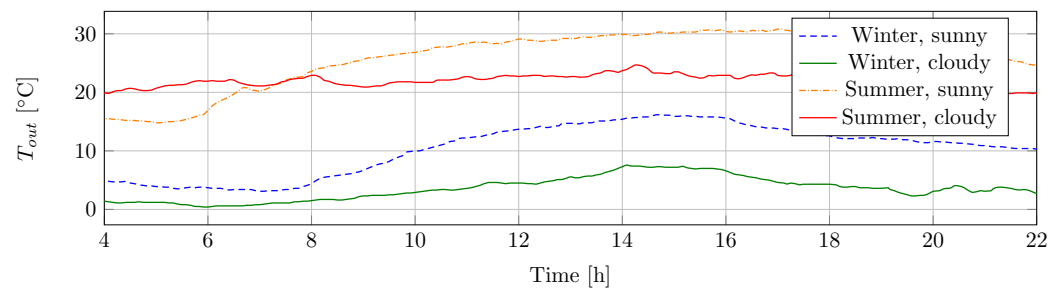
Figure 4. Outer temperature profiles for the four scenarios.

The Almanac of Minutely Power dataset (AMPds) [43] contains electricity, water, and natural gas measurements at one minute intervals for two years of monitoring. There is a total of twenty-one power meters and two water meters installed in a residential house similar to the one analyzed in this study. The 21 electronic submeters were assigned to groups: controllable and noncontrollable devices. Controllable devices consist of the HVAC, heat pump, and hot water heater, and noncontrollable group contains bedroom, basement, dining room plugs and lights, clothes washer and dryer, dishwasher, kitchen fridge and oven, garage, home office, entertainment, utility room, and outside plugs. All noncontrollable measurements were added, and a typical 1 d time series was created by calculating the average value of the same minute for every day of the two-year monitoring period. Figure 5 shows the noncontrollable consumption for all the scenarios ($P_{load}(t)$).
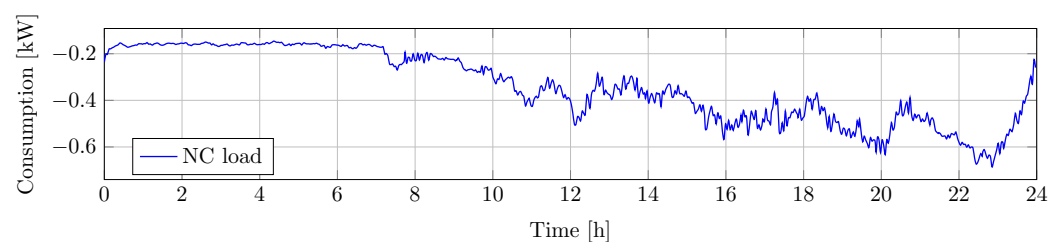

Figure 5. Noncontrollable electrical load for the four different scenarios.

Hot water consumption (Figure 6) was calculated by the same method as the non-controllable load. The Almanac of Minutely Power dataset was the source of the 1 min consumption data. The mean value was calculated for every minute of the day to generate a 1 d normal water consumption ($dm^{cons}_{water}(t)/dt$).
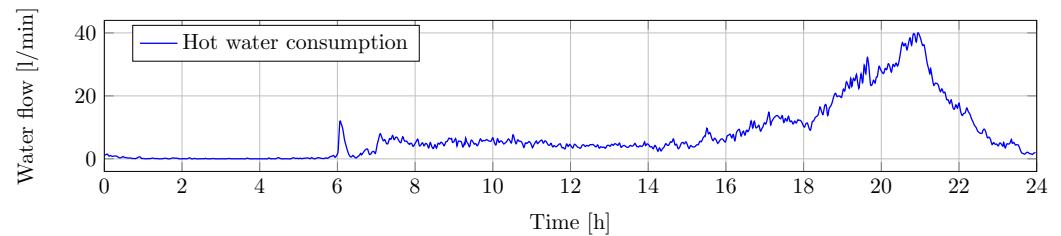

Figure 6. Hot water consumption for the four different scenarios.

3.2. Simulation Results for the Scenarios

3.2.1. Winter—Sunny Day

Figure 7 shows the power consumption and generation of the simulated devices. Supply from the grid and PV generation was the primary sources of energy. Net power is the balance of the house; it is the volume of power consumption from or fed to the grid. When the PV generates sufficient power to feed all consumption units, the energy surplus charges the battery. The greedy battery control method discharges the storage when the PV is low. After 8 p.m., the house is supplied from the grid again, after the battery becomes empty.

The band of flexibility was not symmetric: although the house was a prosumer, generation and storage capacity was limited, and consumption was intermittent. There was more time when a consumption device could be turned on than off, so the downward flexibility was higher. PV generation increased the upward flexibility by charging the battery: the battery consumption could always be switched to production.
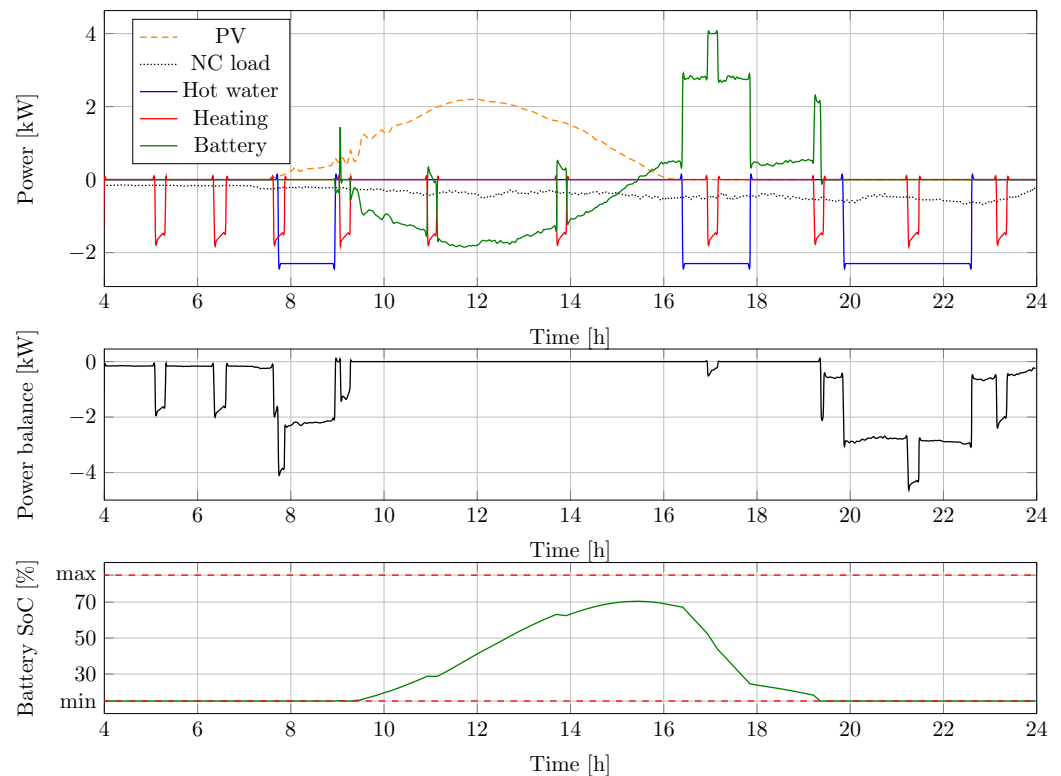

Figure 7. Power consumption/generation of devices for the winter sunny day scenario.

The upward and downward flexibility capabilities of each device were added, resulting in the building's maximum flexible power (Figure 8).
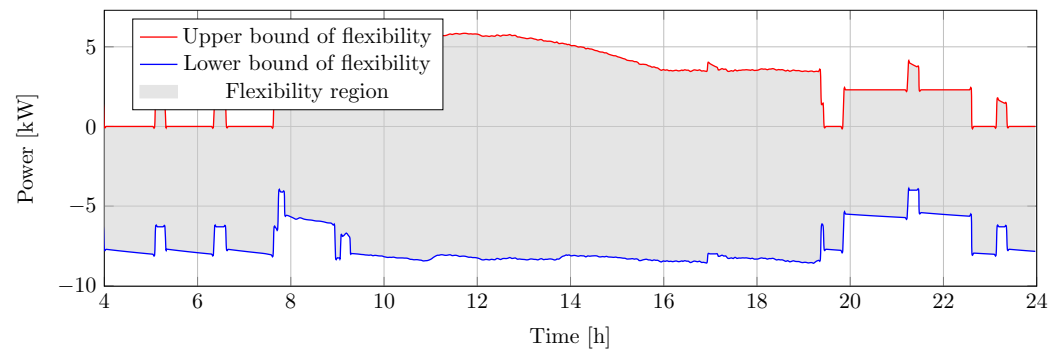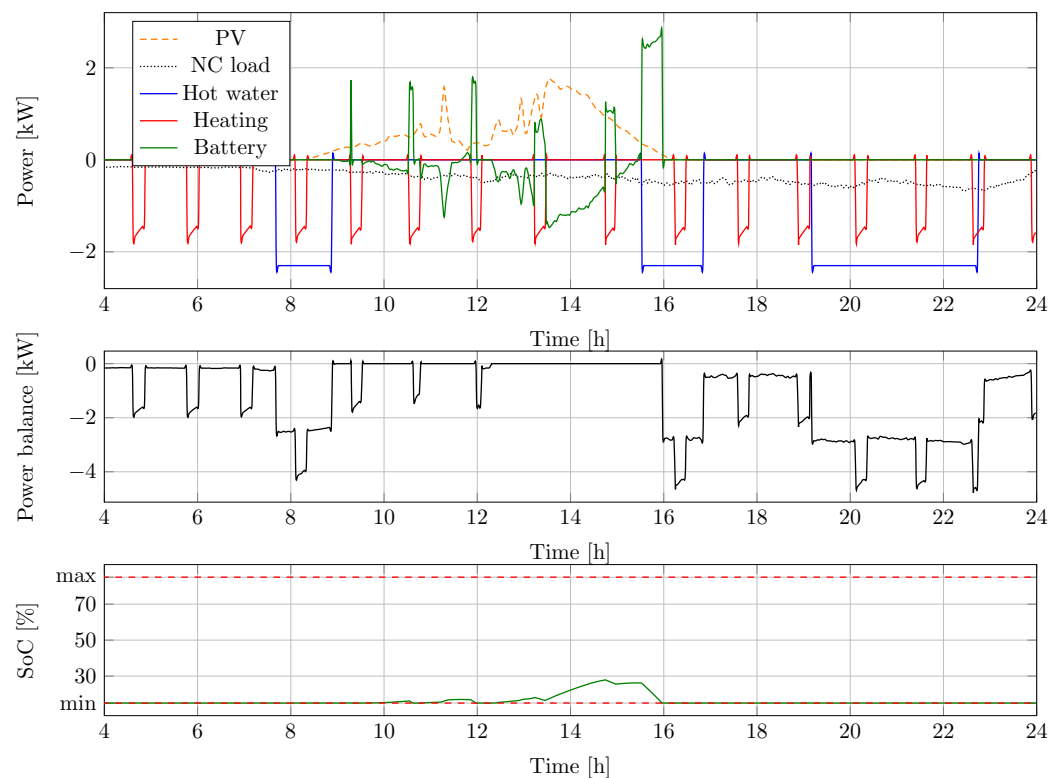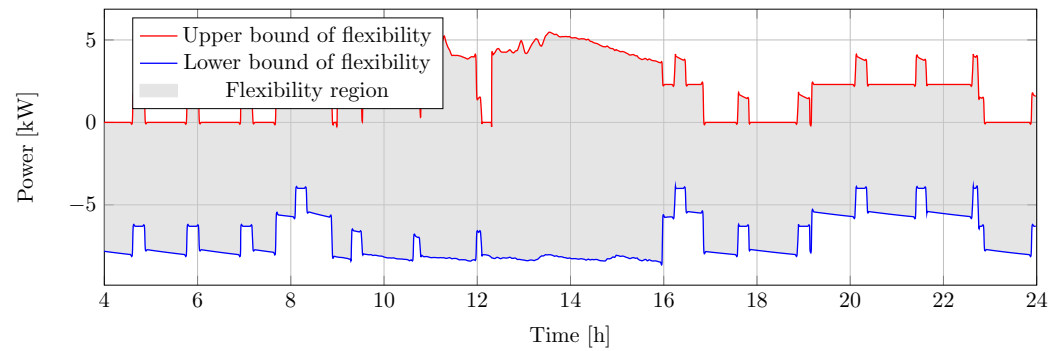

Figure 8. Available upward and downward flexibility for the winter sunny day scenario.

3.2.2. Winter—Cloudy

Figure 9 shows the power consumption and generation of the simulated devices. On a cloudy winter day, the effect of self-generation was limited, and upward flexibility was confined to the short periods when consumption devices operate or the PV is able to supply the house and charge the battery. The downward direction was not affected.

Figure 9. Power consumption/generation of devices for the winter cloudy day scenario.

The upward and downward flexibility capabilities of each device were added, resulting in the building's maximum flexible power (Figure 10).

Figure 10. Available upward and downward flexibility for the winter cloudy day scenario.

3.2.3. Summer—Sunny

Figure 11 shows the power consumption and generation of the simulated devices. On a sunny summer day, the PV generation had a major effect: together with the storage, self-production was sufficient to supply the instantaneous power consumption of the house. After noon, the generation surplus was fed back to the grid.
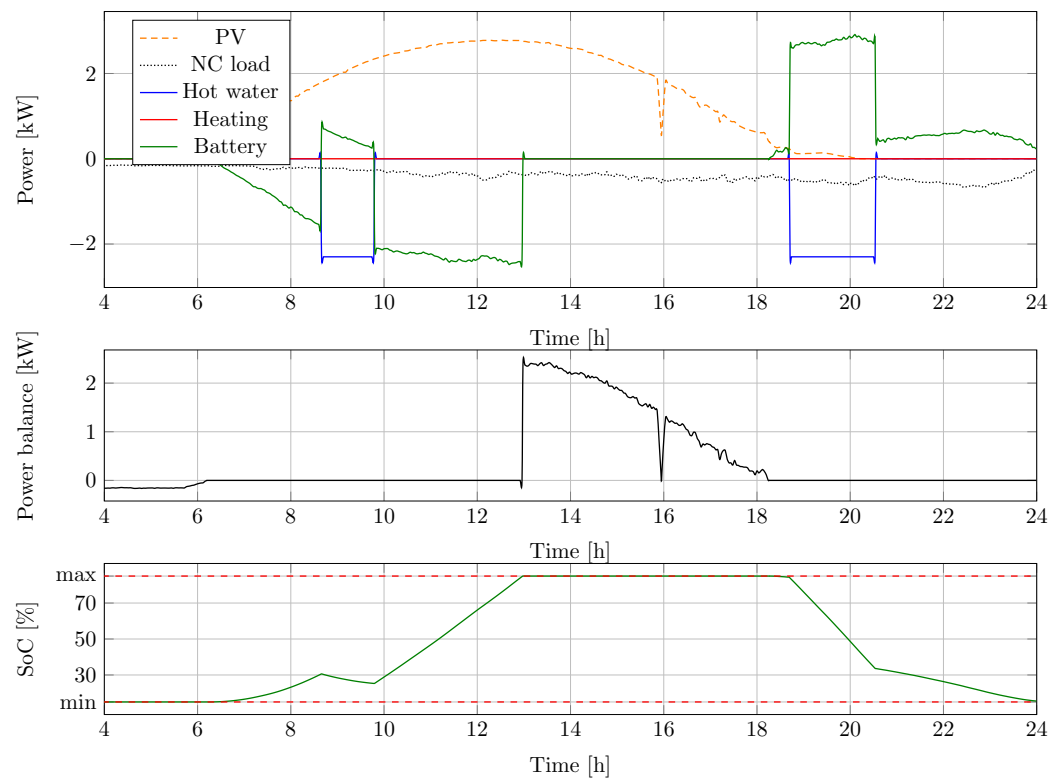

Figure 11. Power consumption/generation of devices for the summer sunny day scenario.

The upward and downward flexibility capabilities of each device were added, resulting in the building's maximum flexible power (Figure 12).

3.2.4. Summer—Cloudy

Figure 13 shows the power consumption and generation of the simulated devices. A cloudy summer day resulted in a more variable upward flexibility in the positive direction. The energy of PV production was not enough to supply the house all day, but 90% of the time, so there was no grid usage.
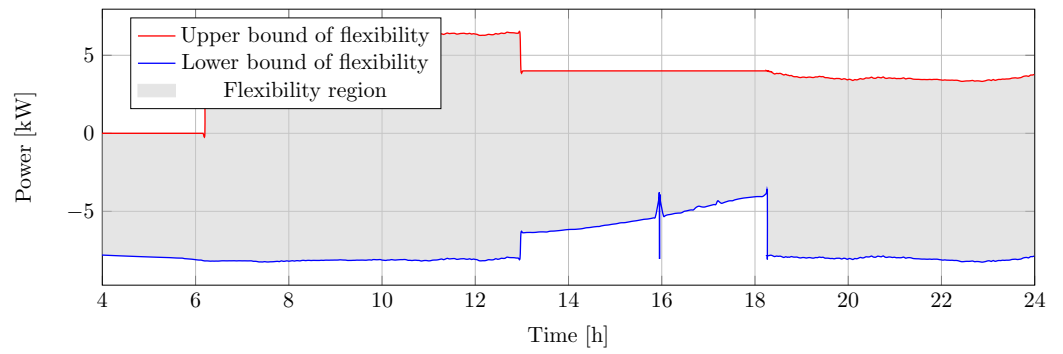
Figure 12. Available upward and downward flexibility for the summer sunny day scenario.
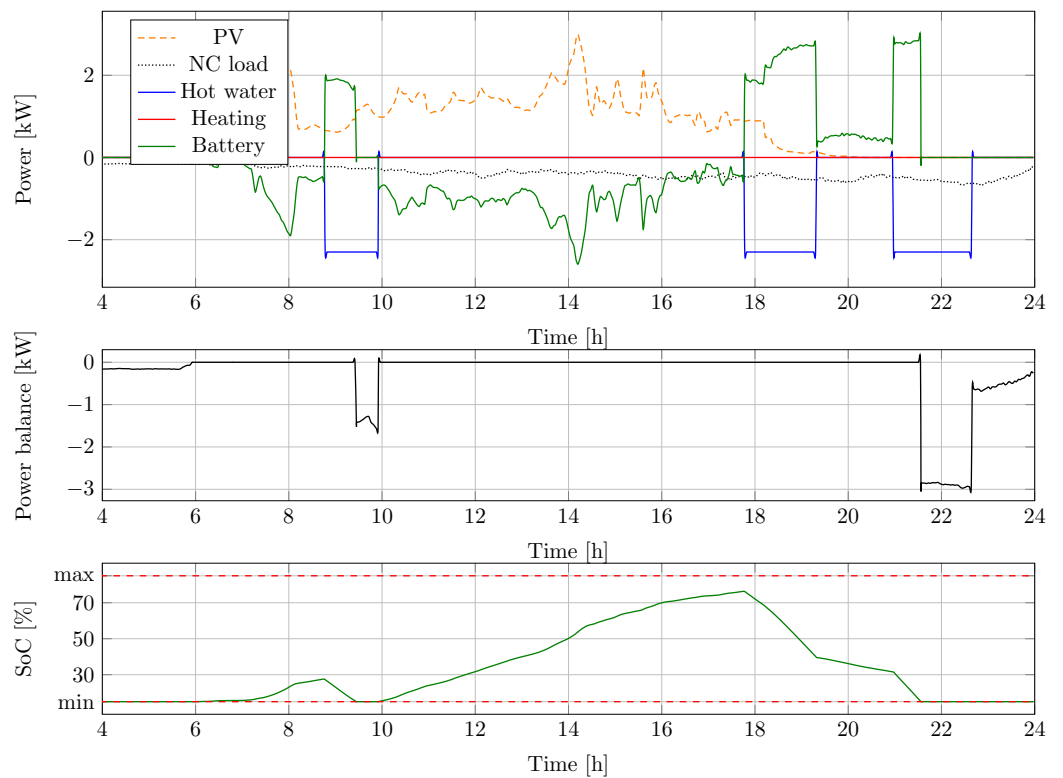

Figure 13. Power consumption/generation of devices for the summer cloudy day scenario.

The upward and downward flexibility capabilities of each device were added, resulting in the building's maximum flexible power (Figure 14).
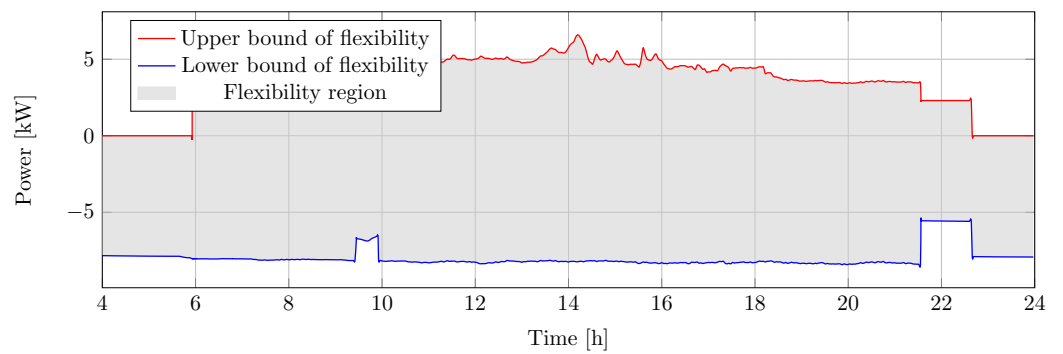

Figure 14. Available upward and downward flexibility for the summer cloudy day scenario.

3.2.5. Prediction

The previous sections presented prosumer flexibility in different environmental conditions for 1 d. Here, the results of the forecast model (Section 2.8) are shown based on one month of one-minute resolution input data for the upward direction. The simulation of the flexibility represents the true value of the target variable. One-third of the one-month input interval was held back as a test to provide an unbiased evaluation of the model fit on the training dataset.

The ridge regression model generates the target variable of the linear forecast model, that is the 15 min forecast of up and down flexibility. Prediction on the test set provided a 25.5% CVRMSE and a 0.89 R2 score. Figure 15 shows a 4 h sample of the prediction.
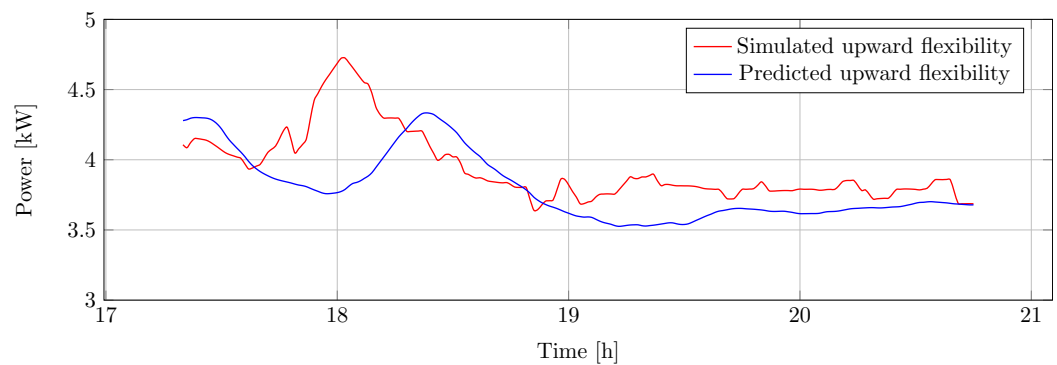

Figure 15. Sample from the upward flexibility prediction between 17:20 and 20:45.

The predictors explained the target variable well; however, the variability of the errors was high given the short forecast interval.

3.3. *Discussion of the Results*

Applying measured weather and load data, the experiments were performed along four different, but typical scenarios. The results showed that the highest range of flexibility was available in the summer time, when there was no heating and the solar generation was maximal. It was also clear that the battery usage was higher in the summer, when the solar generation was not being consumed instantly. It is important to note that a properly sized air conditioner unit would balance the load between the summer and winter periods.

4. Conclusions

Demand-side flexibility can be a valuable source for system operators; however, residential prosumers do not follow a well-defined schedule, so a firm volume of available flexibility cannot be planned, but predicted. A flexibility framework was proposed in this paper for residential prosumers in a distributed generation setup. The residential prosumer of the case study was parameterized so that it described a usual residential actor of the system. To quantify building demand flexibility, the thermoelectric dynamic response of the building energy system was modeled and implemented in MATLAB Simulink. Power consumption and generation were modeled. Simulations were performed based on real world data, and the flexibility potential was calculated for both up and down flexibility. The simulation of four scenarios was executed, which covered one day in different seasons. Power consumption and generation were calculated, as well as upward and downward instantaneous flexibility.

A ridge-regression-based prediction method was designed, and the short-term forecast was calculated. The simulation and prediction experiments showed that the proposed method could serve as the basis of a state estimator or prediction unit. The accuracy of the forecast was moderate, but by assessing different prediction methods on the prosumer flexibility model, we could choose the right tool to improve accuracy and confidence of the prediction.

The aggregation of prosumers' flexibility is necessary to reach the volume that a system operator can utilize. The framework presented forms a basis to analyze the flexibility prediction opportunities on aggregated prosumer portfolios.

The future research directions include the generalization of the method to a higher number of households, for example a local transformer area, in order to give an estimate of the flexibility of a group of prosumers. Another step in the development of the proposed method is to use novel prediction methods from the field of data science to enhance the short-term prediction performance for flexibility.

Abbreviations

The following abbreviations are used in this manuscript:

COP	Coefficient of performance
CVRMSE	Coefficient of variation of the root-mean-squared error
DR	Demand response
DG	Distributed generation
DSM	Demand-side management
DHW	Domestic hot water
EPS	Expanded polystyrene
HEM	Home energy management
HP	Heat pump
HVAC	Heating, ventilating, and air conditioning
PV	Photovoltaic
SoC	State-of-charge
TSO	Transmission system operator
DSO	Distribution system operator

Appendix A

The simulation parameters were taken from the energy audit of a residential building located in Hungary. Together with the house geometry, they are referred to as the "house parameters". The authors determined additional simulation values considering the typical configuration or characteristics of the devices.

Table A1. Simulation parameters.

Parameter	Value	Unit of Measure	Source
l_H	22	m	House parameter
w_H	10	m	House parameter
h_H	3	m	House parameter
n_W	7	m	House parameter
w_W	1	m	House parameter
h_W	1.6	m	House parameter
λ_{Brick}	0.179	W/(m·K)	House parameter
λ_{EPS}	0.035	W/(m·K)	House parameter
d_{Brick}	0.38	m	House parameter
d_{InsW}	0.15	m	House parameter
d_{InsS}	0.3	m	House parameter
$U_{Windows}$	0.9	W/(m²*K)	House parameter
m_{water}	120	kg	Determined by the authors
$T_{water}(0)$	55	°C	Determined by the authors
T_{water}^{sp}	65	°C	Determined by the authors
T_{water}^{th}	15	°C	Determined by the authors
C_{water}	4181	J/(kg·K)	Physical constant
η_{water}	0.9	-	Determined by the authors
P_{water}^{max}	2300	W	Determined by the authors
hl_{water}	0.0069	W/(kg·K)	Derived from the results of [34]
$T_{air}^{indoor}(0)$	24	°C	Determined by the authors
T_{air}^{sp}	22	°C	Determined by the authors
T_{air}^{th}	3	°C	Determined by the authors
$T_{heating}$	50	°C	Determined by the authors
$dm_{air}(t)/dt$	Constant 0.2	kg/s	Determined by the authors
C_{air}	1005.4	J/(kg·K)	Physical constant
ρ_{air}	1.225	kg/m³	Physical constant
$P_{heating}^{max}$	10,000	W	Determined by the authors
$cop_{heating}$	3.6	-	Determined by the authors
$SoC(0)$	15	%	Determined by the authors
$MinSoC$	15	%	Determined by the authors
$MaxSoC$	85	%	Determined by the authors
$P_{battery}^{max}$	4000	W	Determined by the authors
$\eta_{battery}$	0.9	-	Determined by the authors

References

1. Saleh, S.A.; Pijnenburg, P.; Castillo-Guerra, E. Load Aggregation from Generation-Follows-Load to Load-Follows-Generation: Residential Loads. *IEEE Trans. Ind. Appl.* **2017**, *53*, 833–842. [CrossRef]
2. Merino, J.; Gómez, I.; Turienzo, E.; Madina, C. *Ancillary Service Provision by RES and DSM Connected at Distribution Level in the Future Power System*; Technical Report; SmartNet project D: Donostia-San Spain, 2016.
3. Bálint, R.; Fodor, A.; Magyar, A. Model-Based Power Generation Estimation of Solar Panels Using Weather Forecast for Microgrid Application. *Acta Polytech. Hung.* **2019**, *16*, 149–165.
4. Kirbas, I.; Kerem, A. Short-Term Wind Speed Prediction Based on Artificial Neural Network Models. *Meas. Control* **2016**, *49*, 183–190. [CrossRef]
5. Qian, Z.; Pei, Y.; Zareipour, H.; Chen, N. A Review and Discussion of Decomposition-Based Hybrid Models for Wind Energy Forecasting Applications. *Appl. Energy* **2019**, *235*, 939–953. [CrossRef]
6. Gissey, G.C.; Subkhankulova, D.; Dodds, P.E.; Barrett, M. Value of Energy Storage Aggregation to the Electricity System. *Energy Policy* **2019**, *128*, 685–696. [CrossRef]
7. García Vera, Y.E.; Dufo-López, R.; Bernal-Agustín, J.L. Energy Management in Microgrids with Renewable Energy Sources: A Literature Review. *Appl. Sci.* **2019**, *9*, 3854. [CrossRef]
8. European Commission. *Proposal for a Directive of the European Parliament and of the Council on Common Rules for the Internal Market in Electricity*; Council of the European Union: Brussels, Belgium, 2017.

9. Mandatova, P.; Mikhailova, O. *Flexibility and Aggregation: Requirements for Their Interaction in the Market*; Eurelectric: Brussels, Belgium, 2014.
10. McPherson, M.; Tahseen, S. Deploying Storage Assets to Facilitate Variable Renewable Energy Integration: The Impacts of Grid Flexibility, Renewable Penetration, and Market Structure. *Energy* **2018**, *145*, 856–870. [CrossRef]
11. Moura, R.; Brito, M.C. Prosumer Aggregation Policies, Country Experience and Business Models. *Energy Policy* **2019**, *132*, 820–830. [CrossRef]
12. Kubli, M.; Canzi, P. Business Strategies for Flexibility Aggregators to Steer Clear of Being "Too Small to Bid". *Renew. Sustain. Energy Rev.* **2021**, *143*, 110908. [CrossRef]
13. Lezama, F.; Soares, J.; Canizes, B.; Vale, Z. Flexibility Management Model of Home Appliances to Support DSO Requests in Smart Grids. *Sustain. Cities Soc.* **2020**, *55*, 102048. [CrossRef]
14. Zhang, L.; Good, N.; Mancarella, P. Building-to-Grid Flexibility: Modelling and Assessment Metrics for Residential Demand Response from Heat Pump Aggregations. *Appl. Energy* **2019**, *233-234*, 709–723. [CrossRef]
15. Dörre, E.; Pfaffel, S.; Dreher, A.; Girón, P.; Heising, S.; Wiedemann, K. Flexibility Reserve of Self-Consumption Optimized Energy Systems in the Household Sector. *Energies* **2021**, *14*, 3017. [CrossRef]
16. Langevin, J.; Harris, C.B.; Satre-Meloy, A.; Chandra-Putra, H.; Speake, A.; Present, E.; Adhikari, R.; Wilson, E.J.; Satchwell, A.J. US Building Energy Efficiency and Flexibility as an Electric Grid Resource. *Joule* **2021**. [CrossRef]
17. Validzic, D. Clean Energy for All Europeans-European Union's New Legislative Framework. In *Paper Abstracts of 26th Forum: Energy Day in Croatia: European Commission Winter Package—Is It Ambitious Enough to Make Radical Changes on the Energy Market*; Ministry of Environment and Energy of the Republic of Croatia: Zagreb, Croatia, 2017; Volume 32.
18. Borowski, P.F. Digitization, Digital Twins, Blockchain, and Industry 4.0 as Elements of Management Process in Enterprises in the Energy Sector. *Energies* **2021**, *14*, 1885. [CrossRef]
19. Borowski, P.F. Zonal and Nodal Models of Energy Market in European Union. *Energies* **2020**, *13*, 4182. [CrossRef]
20. Xue, L.; Teng, Y.; Zhang, Z.; Li, J.; Wang, K.; Huang, Q. Blockchain Technology for Electricity Market in Microgrid. In Proceedings of the 2017 2nd International Conference on Power and Renewable Energy (ICPRE), Piscataway, NJ, USA, 20–23 September 2017; pp. 704–708. [CrossRef]
21. Shewale, A.; Mokhade, A.; Funde, N.; Bokde, N.D. An Overview of Demand Response in Smart Grid and Optimization Techniques for Efficient Residential Appliance Scheduling Problem. *Energies* **2020**, *13*, 4266. [CrossRef]
22. Bahloul, M.; Majumdar, A.; Daoud, M.; Khadem, S. Energy Storage System: A Potential "Flexibility Resources" to Accelerate the Decarbonisation of Smart Grid Network. In Proceedings of the 12th Mediterranean Conference on Power Generation, Transmission, Distribution and Energy Conversion (MEDPOWER 2020), Online, 9–12 November 2021; pp. 14–20. [CrossRef]
23. Takeshita, T.; Aki, H.; Kawajiri, K.; Ishida, M. Assessment of Utilization of Combined Heat and Power Systems to Provide Grid Flexibility alongside Variable Renewable Energy Systems. *Energy* **2021**, *214*, 118951. [CrossRef]
24. Basaran, K.; Cetin, N.S.; Borekci, S. Energy Management for On-Grid and off-Grid Wind/PV and Battery Hybrid Systems. *IET Renew. Power Gener.* **2017**, *11*, 642–649. [CrossRef]
25. Hopper, N.; Goldman, C.; Neenan, B. Demand Response from Day-Ahead Hourly Pricing for Large Customers. *Electr. J.* **2006**, *19*, 52–63. [CrossRef]
26. Jang, D.; Eom, J.; Kim, M.G.; Rho, J.J. Demand Responses of Korean Commercial and Industrial Businesses to Critical Peak Pricing of Electricity. *J. Clean. Prod.* **2015**, *90*, 275–290. [CrossRef]
27. Shakeri, M.; Pasupuleti, J.; Amin, N.; Rokonuzzaman, M.; Low, F.W.; Yaw, C.T.; Asim, N.; Samsudin, N.A.; Tiong, S.K.; Hen, C.K.; Lai, C.W. An Overview of the Building Energy Management System Considering the Demand Response Programs, Smart Strategies and Smart Grid. *Energies* **2020**, *13*, 3299. [CrossRef]
28. Lopes, R.A.; Chambel, A.; Neves, J.; Aelenei, D.; Martins, J. A Literature Review of Methodologies Used to Assess the Energy Flexibility of Buildings. *Energy Procedia* **2016**, *91*, 1053–1058. [CrossRef]
29. Nuytten, T.; Claessens, B.; Paredis, K.; Van Bael, J.; Six, D. Flexibility of a Combined Heat and Power System with Thermal Energy Storage for District Heating. *Appl. Energy* **2013**, *104*, 583–591. [CrossRef]
30. De Coninck, R.; Helsen, L. Bottom-up Quantification of the Flexibility Potential of Buildings. In Proceedings of the 13th Conference of the International Building Performance Simulation Association, Chambéry, France, 26–28 August 2013; pp. 3250–3258.
31. Xu, X.; Lyu, Q.; Qadrdan, M.; Wu, J. Quantification of Flexibility of a District Heating System for the Power Grid. *IEEE Trans. Sustain. Energy* **2020**, *11*, 2617–2630. [CrossRef]
32. Lucas, A.; Jansen, L.; Andreadou, N.; Kotsakis, E.; Masera, M. Load Flexibility Forecast for DR Using Non-Intrusive Load Monitoring in the Residential Sector. *Energies* **2019**, *12*, 2725. [CrossRef]
33. Sadeghianpourhamami, N.; Demeester, T.; Benoit, D.; Strobbe, M.; Develder, C. Modeling and Analysis of Residential Flexibility: Timing of White Good Usage. *Appl. Energy* **2016**, *179*, 790–805. [CrossRef]
34. Cruickshank, C.A.; Harrison, S.J. Heat Loss Characteristics for a Typical Solar Domestic Hot Water Storage. *Energy Build.* **2010**, *42*, 1703–1710. [CrossRef]
35. ISO 6946:2017. *Building Components and Building Elements: Thermal Resistance and Thermal Transmittance: Calculation Method*; International Organization for Standardization: Geneva, Switzerland, 2017.

36. Kucevic, D.; Tepe, B.; Englberger, S.; Parlikar, A.; Mühlbauer, M.; Bohlen, O.; Jossen, A.; Hesse, H. Standard Battery Energy Storage System Profiles: Analysis of Various Applications for Stationary Energy Storage Systems Using a Holistic Simulation Framework. *J. Energy Storage* **2020**, *28*, 101077. [CrossRef]

37. Kersken, M.; Heusler, I.; Strachan, P. Full Scale Empirical Validation for Building Energy Simulation Programs. In Proceedings of the 9th International Conference on System Simulation in Buildings, Liege, Belgium, 10–12 December 2014.

38. Reynders, G. Quantifying the Impact of Building Design on the Potential of Structural Storage for Active Demand Response in Residential Buildings. Ph.D. Thesis, KU Leuven, Leuven, Belgium, 2015.

39. Rushdi, M.A.; Rushdi, A.A.; Dief, T.N.; Halawa, A.M.; Yoshida, S.; Schmehl, R. Power Prediction of Airborne Wind Energy Systems Using Multivariate Machine Learning. *Energies* **2020**, *13*, 2367. [CrossRef]

40. Yi, Y.; Chen, Y.; Dai, J.; Gui, X.; Chen, C.; Lei, G.; Wang, W. Semi-Supervised Ridge Regression with Adaptive Graph-Based Label Propagation. *Appl. Sci.* **2018**, *8*, 2636. [CrossRef]

41. Ruiz, G.R.; Bandera, C.F. Validation of Calibrated Energy Models: Common Errors. *Energies* **2017**, *10*, 1587. [CrossRef]

42. Montgomery, D.C.; Peck, E.A.; Vining, G.G. *Introduction to Linear Regression Analysis*; John Wiley & Sons: Hoboken, NJ, USA, 2021.

43. Makonin, S.; Ellert, B.; Bajić, I.V.; Popowich, F. Electricity, Water, and Natural Gas Consumption of a Residential House in Canada from 2012 to 2014. *Sci. Data* **2016**, *3*, 160037. [CrossRef] [PubMed]